Transmembrane Helix Association Affinity Can Be Modulated by Flanking and Noninterfacial Residues

Jinming Zhang and Themis Lazaridis*

Department of Chemistry, City College of New York/CUNY, New York, NY 10031

ABSTRACT The GxxxG sequence motif mediates the association of transmembrane (TM) helices by providing a site of close contact between them. However, it is not sufficient for strong association. For example, both bacteriophage M13 major coat protein (MCP) and human erythrocyte protein glycophorin A (GpA) contain a GxxxG motif in their TM domains and form a homodimer, but the association affinity of MCP, measured by the ToxCAT in vivo assay, is dramatically weaker than that of GpA. Even when all interfacial residues of MCP were substituted for those of GpA (MCP-GpA), association remained significantly weaker than in GpA. Here we provide an explanation for these experimental observations using molecular dynamics simulations in an implicit membrane (IMM1-GC). The association free energies of GpA29 (GpA with 29 residues all from the wild-type sequence), GpA15p11 (GpA with 15 residues from the wild-type sequence plus 11 flanking residues from the ToxCAT construct), MCP, and MCP-GpA TM helices were calculated and compared. MCP and MCP-GpA have the same flanking residues used in the ToxCAT assay as those in GpA15p11, but the position of the flanking residues relative to the GxxxG motif is different. The calculated association free energies follow experimental observations: the association affinity of MCP-GpA falls between those of GpA15p11 and MCP wild-type. MCP exhibits an equally strong interhelical interaction in the TM domain. A major reason for the weaker association of MCP in the calculations was the noninterfacial residue Lys-40, which in the dimer structure is forced to be buried in the membrane interior. To alleviate the desolvation cost, in MCP and MCP-GpA dimers, Lys-40 gets deprotonated. A second factor that modulates association affinity is the flanking residues. Thanks to them, GpA15p11 exhibits a much stronger association affinity than GpA29. The positioning of the flanking residues is also important, as evidenced by the difference in association affinity between MCP and MCP-GpA on one hand and GpA15p11 on the other. Thus, residues outside the contact interface can exert a significant influence on transmembrane helix association affinity.

INTRODUCTION

The interaction between transmembrane (TM) helices plays a key role in the structure and function of membrane proteins. It is the second essential step in forming the tertiary structure of multiple-spanning TM proteins according to the two-stage model and its recent refinements (1,2). Moreover, the dynamic interaction between TM helices seems to be involved in crucial cellular processes, such as signal transduction and membrane transport (3,4). The recent computational design of synthetic TM helical peptides to interact with target TM proteins with high selectivity opens new avenues for therapeutic intervention (5). Thus, understanding the rules that govern the association between TM helices is of great importance for membrane protein structure prediction and drug design.

Glycophorin A (GpA), a single-span human erythrocyte protein, is one of the most extensively studied TM helical proteins. The association of the GpA TM domain and its variants has been studied by gel electrophoresis (6,7), analytical ultracentrifugation, and fluorescence resonance energy transfer (FRET) in micelles (8–12), and by the ToxR/ToxCAT/GALLEX system in biological membranes (13–16). Mutagenesis studies on the GpA TM domain have shown the great importance of the sequence motif LIxxGVxxGVxxT, and especially the GxxxG motif, to the stability of the homodimer (6,7,13–15,17,18). Statistical analysis found that the GxxxG motif occurs in membrane proteins at a frequency far above expectation (19). As revealed in both solution and solid-state NMR structures of GpA (20,21), the seven residues on the LIxxGVxxGVxxT motif form a close interhelical packing interface facilitated by the two small glycine residues at the center. It has been proposed that a Cα-H$\cdots$O hydrogen bond network along this motif also contributes significantly to dimer stability (22), an idea confirmed by experiments (23) and computation (24). Computational modeling studies have shown that van der Waals interactions contribute the most to interhelical interaction (25) and association free energy (26,27). More recently, a more extended motif called the glycine zipper, such as (G,A,S)xxxGxxxG and GxxxGxxx(G,S,T), has been identified and found to promote right-handed packing of TM helices (28).

The main emphasis so far in explaining the driving force for TM helix association has been on the residues that form the binding interface. The noninterfacial residues and the residues flanking the 13-residue motif LIxxGVxxGVxxT are widely thought to be unimportant for association affinity because hydrophobic mutations in them had little effect on association affinity (6,10,15,18,29). Nevertheless, substituting noninterfacial residues for polar residues may induce strikingly different results on association affinity, which are difficult to rationalize (6,7,15). To investigate how the affinity of the GxxxG motif is modulated, the association affinities of

Submitted June 27, 2008, and accepted for publication March 3, 2009.

*Correspondence: tlazaridis@ccny.cuny.edu

Editor: Nathan Andrew Baker.

0006-3495/09/06/4418/10 $2.00

doi: 10.1016/j.bpj.2009.03.008

bacteriophage M13 major coat protein (MCP) and GpA were recently compared on the *Escherichia coli* inner membrane by the ToxCat assay (30). Although both GpA and MCP contain a GxxxG motif in their TM domains and form a homodimer, the association affinity of MCP is dramatically weaker than GpA. Even when all of the interfacial residues on MCP were substituted with those from the LIxxGVxxGVxxT motif on GpA, the association affinity of that MCP mutant (MCP-GpA) was significantly weaker than that of GpA. This observation can not be explained by steric clashes or the loss of favorable contacts on the interhelical interface—explanations that worked for most earlier mutagenesis studies (31,32). Another issue that needs to be investigated is whether the flanking residues used in the in vivo constructs (ToxR/ToxCAT constructs) have an influence on the association affinity.

In this article, GpA29 (all 29 residues taken from GpA wild-type sequence), GpA15p11 (15 residues taken from GpA wild-type sequence plus 11 flanking residues from the ToxCAT construct), MCP, and MCP-GpA TM helices are subjected to molecular dynamics (MD) simulations (the sequences are shown in Table 1). All simulations are performed in an implicit zwitterionic membrane model (IMM1) or an implicit anionic membrane model (IMM1-GC). The initial structures of MCP and MCP-GpA dimers were modeled based on the solid-state NMR structure of GpA (21) because previous work showed that the structures of MCP and GpA are very similar (30). First, the protonation state of Lys-40 in MCP and MCP-GC monomers and dimers is investigated in both neutral and anionic membranes. Second, the average configurations and dimer stability of these four sequences during MD simulations are analyzed and compared. Finally the interhelical interactions and association free energies of these helices are calculated and compared to reveal the influence of flanking residues from ToxCAT constructs and noninterfacial residue Lys-40 on the association affinity.

METHODS

IMM1 and IMM1-GC models

This work uses the implicit membrane models, IMM1 and IMM1-GC (33,34). IMM1 is an extension of the implicit aqueous model EEF1 (35). The effective energy (W_{IMM1}) of a protein in a heterogeneous membrane-water system is the sum of the intramolecular energy (E) of the protein and the solvation free energy (ΔG^{slv}) (33),

$$W_{\mathrm{IMMI}} = E + \Delta G^{\mathrm{slv}}. \quad (1)$$

The CHARMM 19 polar hydrogen energy function is used to calculate the intramolecular energy. Contributions from each atom or group i are summed up to calculate the solvation energy,

$$\Delta G^{\mathrm{slv}} = \sum_i \Delta G_i^{\mathrm{slv}} = \sum_i \Delta G_i^{\mathrm{ref}} - \sum_i \sum_{j\neq i} f_i(r_{ij}) V_j. \quad (2)$$

In Eq. 2, $\Delta G_i^{\mathrm{ref}}$ signifies the solvation free energy of group i in a small model compound, and the last term represents the solvation free energy lost as a result of exclusion of solvent by surrounding atoms. In addition, EEF1 uses linear distance-dependent dielectric screening and a net neutral version of the ionizable side chains. In IMM1 the reference solvation free energy depends on the position of each atom with respect to the membrane center and is a linear combination of parameters pertaining to water and to cyclohexane.

$$\Delta G_i^{\mathrm{ref}}(z') = f(z')\Delta G_i^{\mathrm{ref\cdot water}} + (1 - f(z'))\Delta G_i^{\mathrm{ref\cdot cyclohexane}}, \quad (3)$$

where $z'=|z|/(T/2)$ (T is the thickness of hydrophobic core of the membrane), and $f(z')$ is defined by:

$$f(z') = \frac{z'^n}{1 + z'^n}. \quad (4)$$

The value 10 for n gives the appropriate steepness of the transition between nonpolar and polar environments (33). At the hydrocarbon-polar headgroup interface f equals 0.5.

In IMM1 the dielectric screening function also depends on the position with respect to the membrane:

$$\varepsilon = r^{fij}. \quad (5)$$

An empirical model is employed for f_{ij},

$$f_{ij} = 0.85 + 0.15\sqrt{f_i f_j}, \quad (6)$$

where f_i and f_j are given by Eq. 4.

For negatively charged membranes, such as the inner membrane of *Escherichia coli*, a Gouy-Chapman (GC) term is added to W_{IMM1}. The resulting model is called IMM1-GC model, in which the effective energy is named $W_{\mathrm{IMM1\text{-}GC}}$ (34),

$$W_{\mathrm{IMMI-}GC} = W_{\mathrm{IMMI}} + E_{\mathrm{GC}}. \quad (7)$$

E_{GC} is defined as

$$E_{\mathrm{GC}} = \sum_i \psi(z_i) q_i, \quad (8)$$

TABLE 1 The sequences studied in this work

Name	Sequence
GpA29	ACE GLU PRO GLU ILE THR **LEU ILE ILE PHE GLY VAL MET ALA GLY VAL ILE GLY THR ILE LEU** LEU ILE SER TYR GLY ILE ARG ARG LEU CBX
GpA15p11	ACE ASN ARG ALA ARG **LEU ILE ILE PHE GLY VAL MET ALA GLY VAL ILE GLY THR ILE LEU** LEU ILE LEU ILE ASN PRO SER CBX
MCP	ACE ASN ARG ALA ARG TYR ILE GLY TYR **ALA TRP ALA MET VAL VAL VAL ILE VAL GLY ALA THR ILE GLY ILE LYS LEU PHE** LEU ILE LEU ILE ASN PRO SER CBX
MCP-GpA	ACE ASN ARG ALA ARG TYR ILE GLY TYR **ALA TRP ALA MET VAL *LEU* ILE *ILE* VAL GLY *VAL* THR ILE GLY *VAL* LYS LEU *THR*** LEU ILE LEU ILE ASN PRO SER CBX

Residues in bold are those on the putative TM domain adopted from GpA or MCP wild-type sequence. Flanking residues (39) are underlined. Mutated residues are in italics.

where $\psi(z_i)$ is the electrostatic potential generated by a uniformly charged surface at position z_i according to GC theory, and q_i is the partial charge on atom i. *E. coli* membranes contain ~25% anionic lipids (36). Although the distribution of anionic lipids between the two leaflets of the inner membrane has not been firmly established (37), it is likely that the periplasmic side contains a significant fraction (36). In fact, this is often cited as a reason for the selectivity of cationic antimicrobial peptides for bacterial membranes (38). In this work we used a 20% anionic fraction on both sides of the membrane.

MD simulations

The sequences of GpA29, GpA15p11, MCP, and MCP-GpA shown in Table 1 were subjected to MD simulations. GpA29 and GpA15p11 differ only in the flanking residues surrounding the TM domain (residues 75–89 adopted from GpA wild-type sequence), and they were selected to investigate whether these flanking residues affect association affinity. GpA29 has the original flanking residues as wild-type GpA, whereas GpA15p11, MCP, and MCP-GpA all have the same flanking residues generated from restriction sites or ToxR′ domains in a ToxCAT assay (39). The solid-state NMR structure of GpA determined in lipid bilayers (21) was used as the initial structure for MD simulations. Because both molecular modeling and systematic substitution studies have shown that GpA and MCP TM helices have a similar GxxxG-mediated interhelical interface and structural features (30), the initial structures of MCP and MCP-GpA were modeled from the solid-state NMR structure of GpA by structure threading. All the sequences were blocked by the acetyl group (ACE) and the methyl amide group (CBX) at the N- and C-termini, respectively. The initial structures were energy-minimized with 800 steps using the Adopted Basis Newton-Raphson method before MD simulations were performed. Because the association energy is calculated as the small difference between large numbers, strategies for reducing the uncertainty in the energies would be useful. The TM segments of GpA and MCP are mainly α-helical (20,21,30,40); thus, the backbone dihedral angles ϕ and ψ were constrained (force constant 100.0) at the ideal values, -57° and -47°, respectively, to reduce energy fluctuations and thus the error bars. Backbone dihedral angle constraints were found to give lower average effective energies than NOE constraints. The thickness of the membrane hydrophobic core and the smeared charge offset from the hydrocarbon boundary were set to be 26 Å and 3 Å, respectively. All simulations were conducted at 298.15 K with the CHARMM package and the NOSE integrator. For a dimer, the simulation was first performed under BESTFIT constraints, which are similar to the absolute positional constraints except that the reference structure is allowed to rotate and translate so as to best fit the selected atoms and minimize the restraint energy, on the backbone atoms (force constant 1.0) for 0.25 ns for equilibration before the production simulation stage. The monomers were directly subjected to simulations for the production stage. The average structural, configurational, and energetic properties, including the root mean-square deviation (RMSD) and the crossing angle of dimers, the translation on the Z axis, the tilt angle relative to the membrane normal, and the orientation about the helical axis of the GxxxG motif, effective energies, and interhelical interactions were calculated from the last 0.9 ns of the 1-ns simulations as in previous work if the simulation length is not explicitly indicated (27). As a test of the convergence of the results we also conducted 5-ns simulations, one of which was extended to 10 ns. The rotation of the helix is defined by three Euler angles, which are the angles rotating about X axis (helical axis), Y axis, and Z axis from a reference state (27).

Determination of lysine ionization state

Lys-40 on the TM domain of MCP and MCP-GpA dimers points toward the membrane interior. This could shift its pKa sufficiently to change its ionization state. Thus, the ionization state of Lys-40 in the monomer and the dimer should be determined. With protonated Lys-40 taken as the reference state, the deprotonation energy, $\Delta G_{\text{deprotonation}}$, in a monomer and a dimer can be calculated by the equation (41):

$$\Delta G_{\text{deprotonation}} = -2.303\text{RT}(\text{pH}-\text{pKa}) + \left[\left(W_{\text{Protein-Membrane-Lys}} - W_{\text{Protein-Membrane-Lys+}}\right) - \left(W_{\text{Model-Water-Lys}} - W_{\text{Model-Water-Lys}}\right)\right], \tag{9}$$

where the pH and the pKa of lysine in water are taken as 7.0 and 10.53, respectively. $W_{\text{Protein-Membrane-Lys}}$ and $W_{\text{Protein-Membrane-Lys+}}$ are average effective energies of a protein (either a monomer or a dimer) in the membrane with Lys-40 deprotonated and protonated, respectively. Simulations of deprotonated and protonated forms of monomers and dimers were performed separately using the IMM1 and IMM1-GC models to calculate $W_{\text{Protein-Membrane-Lys}}$ and $W_{\text{Protein-Membrane-Lys+}}$. $W_{\text{Model-Water-Lys}}$ and $W_{\text{Model-Water-Lys+}}$ are average effective energies in a model compound where the lysine is deprotonated and protonated, respectively, and fully exposed to aqueous solution. A short peptide, ACE-ALA-ALA-LYS-ALA-ALA-CBX, in extended conformation was used as the model compound. $W_{\text{Model-Water-Lys}}$ and $W_{\text{Model-Water-Lys+}}$ were calculated from 10-ns simulations in EEF1 with all residues except lysine fixed. If $\Delta G_{\text{deprotonation}} < 0$, then the deprotonated state is more favorable. The pKa shift is the quantity in brackets in Eq. 9 divided by 2.303RT.

Association free energy calculations

The standard association free energy was calculated at 1 M in hydrophobic phase (HP) standard state, as previously (27). The standard association free energy (ΔG^0_{HP}) can be decomposed into free energy on change in ionization state (ΔG_{ion}), effective energy change on association (ΔW_{ass}), translational entropy loss ($\Delta S^{\text{trans}}_{\text{ass}}$), rotational entropy loss ($\Delta S^{\text{rot}}_{\text{ass}}$), and conformational entropy loss ($\Delta S^{\text{conf}}_{\text{ass}}$):

$$\Delta G^0_{\text{HP}} = \Delta G_{\text{ion}} + \Delta W_{\text{ass}} - T\Delta S^{\text{trans}}_{\text{ass}} - T\Delta S^{\text{rot}}_{\text{ass}} - T\Delta S^{\text{conf}}_{\text{ass}}. \tag{10}$$

The first term was added because of Lys-40 in the TM domain of MCP and MCP-GpA, which can have different ionization states in the monomer and the dimer. For example, if Lys-40 prefers the protonated state in the monomer and the deprotonated state in the dimer, the overall dimerization process can be described as a thermodynamic cycle:

$$\begin{array}{ccc} & \overset{\text{Association II}}{} & \\ 2\ \text{MCP monomers(Lys}^+\text{)} & \rightarrow & \text{MCP dimer(Lys}^+\text{)} \\ \downarrow_{\text{Deprotonation I}} & & \downarrow_{\text{Deprotonation II}} \\ 2\ \text{MCP monomers(Lys)} & \rightarrow & \text{MCP dimer(Lys)}. \\ & \underset{\text{Association I}}{} & \end{array} \tag{11}$$

The overall dimerization energy can be calculated by pathway I or pathway II. The effective energies during the last 0.9 ns of three 1-ns MD simulations of monomers and dimers in the IMM1-GC model were averaged and used to calculate ΔG_{ion} and ΔW_{ass}. Because the constraints on backbone dihedral angles generate an artificial additional energy term, this energy term was subtracted from the total energies. The magnitude of this term was ~28 kcal/mol and ~15 kcal/mol for the dimer and the monomer, respectively. The calculation of the entropic terms is the same as in previous work (27). Briefly, the helices were treated as rigid rods. Translational entropy was calculated from the probability distribution of the center of the rigid body in the X-Y (membrane) plane and on the Z axis (membrane normal). Rotational entropy was calculated from the probability distribution of the three Euler angles that define the orientation of the rigid rod. Side-chain conformational entropy was calculated from the probability distribution of each dihedral angle. The membrane hydrophobic core thickness was set to 26 Å to

mimic the biological membrane where the association affinities of GpA, MCP, and MCP-GpA were compared.

RESULTS

Initial dimer structures

The solid-state NMR structure of GpA (21) was used as the initial structure of GpA29 and GpA15p11 dimers. The initial structures of MCP and MCP-GpA dimers were modeled from the solid-state NMR structure of GpA (21) by structure threading, based on the modeling results of Melnyk et al. (30) Fig. 1 shows the initial structures of GpA15p11 and MCP dimers. Although GpA15p11 and MCP have the same type of flanking residues from the ToxCAT constructs, the 13-residue GxxxG association core is closer to the N-flank in GpA15p11, whereas it is near the middle in MCP.

Ionization states of Lys-40 in the monomer and dimer of MCP and MCP-GpA

In the model of the MCP and MCP-GpA dimers, Lys-40 points toward the membrane interior. This environment can induce large pKa shifts. Thus, the preferred ionization states of Lys-40 in the monomer and dimer should be determined first. With the protonated state taken as the reference state, deprotonation energies of MCP and MCP-GpA monomers and dimers in IMM1 and IMM1-GC membranes were calculated from separate simulations of the monomer and the dimer with protonated/deprotonated Lys-40. The results are shown in Table 2.

The deprotonation energy of MCP and MCP-GpA dimers is highly favorable in both membrane types. (The deprotonation energy of the MCP dimer in IMM1 could not be calculated because three MD runs of the protonated MCP dimer could not maintain the dimer structure, whereas the deprotonated MCP dimer was stable. This suggests that the deprotonation energy for MCP is also highly favorable). The deprotonation energies of Lys-40 in IMM1-GC for the MCP dimer and MCP-GpA dimer are −9.5 kcal/mol and −13.3 kcal/mol, respectively, which correspond to pKa shifts of −10.50 and −13.28, respectively. The deprotonation energies of MCP and MCP-GpA monomers are slightly negative in IMM1 and positive in IMM1-GC, apparently because of the negative charge of the membrane in the latter. This is consistent with the experimental determination by FRET that Lys-40 is located near the hydrophobic and hydrophilic interface and seems to be protonated when the MCP monomer is embedded in an anionic bilayer (42). Therefore, the dimerization process in IMM1-GC includes two steps, and it can be represented by the thermodynamic cycle in Eq. 11, compared with only one step in IMM1.

TABLE 2 Deprotonation energies (kcal/mol) of MCP and MCP-GpA monomers and dimers calculated from 1-ns MD simulations using the IMM1 and IMM1-GC models

		IMM1	IMM1-GC
MCP	Monomer	−0.3	2.1
	Dimer	NA	−9.5
MCP-GpA	Monomer	−1.1	2.2
	Dimer	−18.0	−13.3

The average energy of the protonated MCP dimer in IMM1 was not calculated because none of three runs was able to maintain the dimer structure. The average energies of protonated dimers in IMM1-GC were calculated from one run because two out of three runs were not stable. The other values were calculated from three runs. Equation 9 was used to calculate ionization/deprotonation energy for the monomer and dimer.

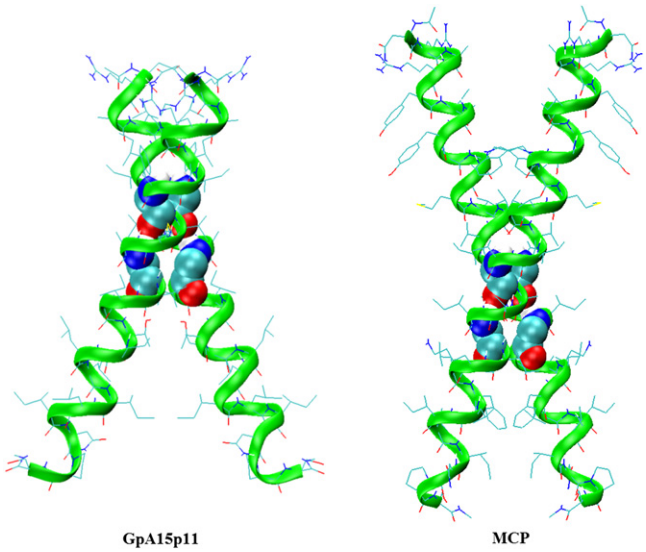

FIGURE 1 The initial dimer structures of GpA15p11 and MCP. Two glycines in GxxxG motif are shown in ball representation.

Configuration of monomers and dimers in the anionic membrane

For each dimer of the GpA29, GpA15p11, MCP, and MCP-GpA sequences, three 1-ns MD simulations were performed in IMM1-GC, starting with a different random number for the assignment of velocities. For the MCP and MCP-GpA dimers, only the deprotonated state of Lys 40 was considered. As shown in Table 3, the average backbone RMSDs of GpA29, GpA15p11, MCP, and MCP-GpA dimers with respect to their initial structures are 1.1 Å, 1.2 Å, 2.0 Å, and 1.5 Å, respectively, which indicates that dimers are sufficiently stable during the simulations. Moreover, plots of backbone RMSD versus time (not shown) show that the backbone RMSDs of GpA29, GpA15p11, MCP, and MCP-GpA never exceed 2.5 Å, 2.5 Å, 4.5 Å, and 3.5 Å, respectively. Table 3 also shows the average crossing angles of the dimers during the simulations, which are 39°, 42°, 46°, and 42°, respectively. Even though the flanking residues of GpA29 and GpA15p11 sequences are dramatically different, there is almost no difference between their average dimeric structures. The average crossing angle of MCP in our simulations is somewhat larger than the value of ~40° predicted

TABLE 3 Structures and configurations in the IMM1-GC membrane model

Structural properties of dimers								
Sequence		GpA29		GpA15p11		MCP		MCP-GpA	
RMSD (Å)		1.1		1.2		2.0		1.5	
Crossing angle (°)		39		42		46		42	
Configuration of a helix as a monomer or in a dimer									
Sequence		GpA29		GpA15p11		MCP		MCP-GpA	
		Helix A	Helix B	Helix A	Helix B	Helix A	Helix B	Helix A	Helix B
Translation(Å)	Monomer+					−4.2	−4.3	−4.1	−4.0
	Monomer	1.3	1.2	3.0	2.9	−0.2	−0.2	−0.4	−0.3
	Dimer	0.4	0.5	2.7	2.8	−0.1	0.2	−0.2	−0.3
Tilt angle(°)	Monomer+					41.2	41.5	40.6	39.7
	Monomer	16.5	15.3	21.0	21.2	23.0	24.6	25.8	23.3
	Dimer	22.5	23.9	25.7	24.2	27.9	27.4	25.6	25.6
Orientation(°)	Monomer+					317.3	317.3	315.1	313.0
	Monomer	170.7	160.7	127.7	143.0	231.8	239.7	249.2	238.5
	Dimer	221.7	226.1	216.1	214.7	214.8	214.8	216.0	213.1

The average RMSD, crossing angle, translation on *Z* axis, tilt angle, and orientation about the helix axis were calculated from the last 0.9 ns of 1-ns MD simulations. Helices A and B are two helices that form a dimer. The protonated monomer is denoted as "Monomer+".

(30), perhaps because a longer MCP sequence and different energy function were used in our study. As expected, MCP-GpA has a structure more similar to GpA15p11 than MCP does, in terms of RMSD and average crossing angles.

To describe the configuration relative to membrane, we calculated the translation of the center of the 13-residue association core on the *Z* axis (which coincides with the membrane normal), the tilt angle of the helix relative to the membrane normal, and the orientation about the helical axis of the 13-residue association core. The configurations of different TM helices were compared and the change in their configurations upon association was examined (shown in Table 3 and Fig. 2). GpA29 and GpA15p11 are similar in the tilt and orientation of helices in the dimer but significantly different in the translation of the monomer and dimer, the tilt angle of the monomer, and the orientation of the monomer. The translation, tilt angle, and orientation of MCP and MCP-GpA are dramatically different for the protonated and deprotonated monomers. On protonation, the monomers of MCP and GpA translate ~4.0 Å down toward the membrane boundary, tilt ~18° more away from membrane normal, and rotate ~80° about the helical axis. These changes allow protonated Lys-40 to reach the membrane-water interface (Fig. 2). The average position of the Lys-40 mass center on both MCP and MCP-GpA is ~−12.0 Å for protonated monomer, ~−5.8 Å for deprotonated monomer, and ~−4.6 Å for deprotonated dimer. For all four sequences, the change of the translation and tilt angle from the uncharged monomer to the dimer was relatively small; however the change of orientation was considerable. Thus different flanking residues and ionizable residues in the TM domain could induce large configurational changes of TM helices in the membrane.

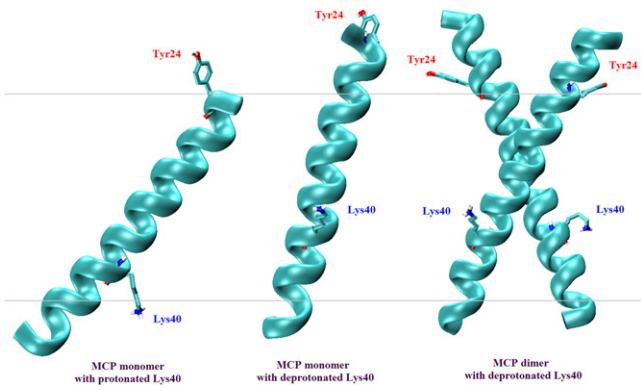

FIGURE 2 Change of configuration of MCP wild-type on association. Residues Tyr-24 and Lys-40 are shown in stick representation.

Interhelical interactions in the anionic membrane

Average interhelical interactions of the four sequences in the IMM1-GC model are shown in Table 4. Surprisingly, the

TABLE 4 Average interhelical interactions (kcal/mol) in the IMM1-GC model calculated from three independent runs of 1-ns MD simulations

	Interhelical interactions	ΔInterhelical interactions
GpA29	−21.2 ± 0.3	+6.5 ± 0.6
GpA15p11	−27.7 ± 0.5	
MCP	−22.3 ± 0.4	+5.4 ± 0.6
MCP-GpA	−25.7 ± 0.3	+2.0 ± 0.6
GpA29 (13 residues)	−16.8 ± 0.2	+1.3 ± 0.2
GpA15p11 (13 residues)	−18.1 ± 0.1	
MCP (13 residues)	−17.4 ± 0.9	+0.7 ± 0.9
MCP-GpA (13 residues)	−20.4 ± 0.3	−2.3 ± 0.3
GpA15p11 (Asn-1–Arg-2)	−2.7 ± 0.7	
MCP (Asn-1–Arg-2)	0.0	+2.7 ± 0.7
MCP-GpA (Asn-1–Arg-2)	0.0	+2.7 ± 0.7

GpA15p11 is used as the reference to calculate Δinterhelical interactions. Errors are standard deviations of the mean from three separate runs.

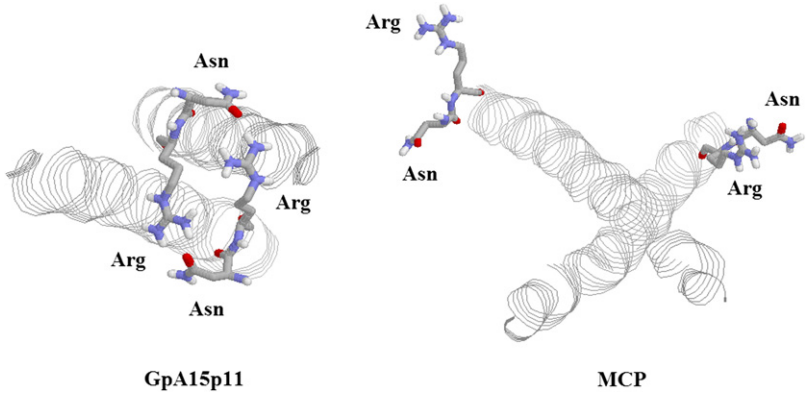

FIGURE 3 Distance between Asn and Arg from the N-flanks of GpA15p11 and MCP dimers. Residues Asn and Arg from the N-flanks are shown in stick representation.

average interhelical interaction of GpA15p11 is ~6.5 kcal/mol stronger than that of GpA29. The two sequences differ only in the flanking residues. The effect could be direct or indirect; i.e., the flanking residues could increase the interhelical interaction between the LIxxGVxxGVxxT motifs because of slight structural and configurational changes induced, or they could directly participate in interhelical interactions. To distinguish between the two possibilities, interhelical interactions between the 13-residue motifs on different helices were calculated. This interaction was found to be only ~1.3 kcal/mol weaker in GpA29 than in GpA15p11. The remainder must be caused by direct interactions between flanking residues. The GpA15p11 flanking residues on the N-terminus, especially the first two residues Asn-1 and Arg-2, could be the major contributors because 1), they are separated from the LIxxxGxxxGxxxT motif by only three and two residues, respectively, and this places them near the interhelical interface; and 2), they are strong H-bond donors or acceptors. In fact, a strong interaction between Asn-1 from one helix and Arg-2 from the other helix was observed in GpA15p11, and the average interaction between them during the simulations was −2.7 kcal/mol. When two pairs of Asn-1 and Arg-2 are considered, their contribution to interhelical interaction is doubled to −5.4 kcal/mol. Hence, flanking residues could participate in interhelical interactions and affect association affinities.

Consistent with observations from prior experiments (30), the interhelical interaction of GpA15p11 is much stronger than that of MCP, and the interhelical interaction of MCP-GpA is between those of GpA15p11 and MCP. However, when we include only the 13 residues corresponding to the LIxxxGxxxGxxxT motif, the interhelical interaction of MCP is close to that of GpA15p11, and the interhelical interaction of MCP-GpA is 2.3 kcal/mol stronger. Therefore, MCP is not a weak scaffold in terms of interhelical interactions from the 13-residue interfacial core compared to GpA. The stonger interhelical interactions in GpA15p11 must be caused by the flanking residues. Although both MCP and MCP-GpA have the same flanking residues as GpA15p11, Asn-1 and Arg-2 in MCP are nine residues further away from the 13-residue interfacial core compared with those in GpA15p11, so these two residues in MCP are not close enough to form H-bonds (Fig. 3). This is supported by the negligible interaction between Asn-1 and Arg-2 from different helices in MCP and MCP-GpA (Table 4).

Standard free energies on association in the anionic membrane

Table 5 summarizes the results for the calculation of standard free energies of the four sequences on association in the IMM1-GC model. Because for MCP and MCP-GpA Lys-40 prefers to be protonated in a monomer and deprotonated in a dimer, the association free energy includes the free energy of deprotonation of the monomers and the association free energy of deprotonated monomers (see two steps of pathway I in Eq. 11). The effective energy changes on deprotonation are +2.1 ± 1.1 kcal/mol and +2.2 ± 1.6 kcal/mol for MCP and MCP-GpA, respectively. The standard association free energies of GpA29, GpA15p11, MCP, and

TABLE 5 Standard free energies (kcal/mol) on association in the IMM1-GC model at 1 M (in HP) standard state

	GpA29	GpA15p11	MCP	MCP-GpA
$\Delta G_{\text{deprotonation}}$			4.2 ± 1.1	4.4 ± 1.6
ΔW_{ass}	−17.1 ± 0.8	−22.4 ± 1.5	−17.4 ± 1.9	−24.6 ± 2.5
$\Delta S_{\text{ass}}^{\text{trans}} \bullet T$	−2.2	−2.0	−2.1	−2.5
$\Delta S_{\text{ass}}^{\text{rot}} \bullet T$	−2.6	−2.5	−3.0	−2.8
$\Delta S_{\text{ass}}^{\text{conf}} \bullet T$	−5.9	−4.9	−3.2	−3.4
ΔG^0 at 1 M (in HP) standard state	−6.5 ± 0.8	−13.0 ± 1.5	−4.9 ± 2.2	−11.4 ± 3.0

The temperature T is 298.15 K. $\Delta G_{\text{deprotonation}}$ is twice that in Table 2 on account of two monomers. Error bars are standard deviations of the mean from three separate runs.

MCP-GpA are -6.5 ± 0.8 kcal/mol, -13.0 ± 1.5 kcal/mol, -4.9 ± 1.9 kcal/mol, and -11.4 ± 2.5 kcal/mol, respectively, so the association affinity of MCP-GpA is between those of GpA15p11 and MCP, as observed experimentally.

Effect of simulation length

Three 5-ns MD simulations were performed for each sequence to investigate the influence of simulation length on the calculated effective energy changes on association. The structure of the GpA15p11 and MCP-GpA (protonated) dimers was stable during all 5-ns MD simulations. One simulation of GpA15p11 was extended to 10 ns, and the dimer remained stable. The dimers of GpA29 and MCP (protonated) were less stable, and their structure was disrupted at some point (3.0 ns, 1.0 ns, and 2.5 ns for GpA29 and 4.5 ns, 5.0 ns, and 4.0 ns for MCP). In this case, the dimers did not dissociate but formed alternative dimeric structures (mostly with parallel helices) with lower effective energy. These structures were stabilized by interactions involving Arg residues outside the membrane. Given the uncertainties in modeling Arg interactions (see Discussion), it is likely that these structures are formed as a result of deficiencies in the effective energy function. Thus, the effective energies of GpA29 and MCP (protonated) dimers were calculated only over the time that the dimer structure was stable. The results are shown in Table 6. The average effective energies of monomers and dimer of each sequence change slightly between 1 ns and the longer simulations (the largest difference <1.7 kcal/mol). The observed differences are similar to the error bars calculated from the 1-ns simulations. Thus, the simulation length should not affect the conclusions drawn from the 1-ns simulations.

DISCUSSION AND CONCLUSIONS

The main conclusions of these calculations are the following: 1), a residue can influence association affinity without being

TABLE 6 Effective energies and effective energy changes on association calculated from 1.0-ns and longer simulations in the IMM1-GC model

Sequence	Length	Molecule	Run No.1	Run No.2	Run No.3	Average
GpA29	1-ns simulations	$W_{\text{Monomer A}}$	−529.7	−529.6	−530.4	−529.9 ± 0.3
		$W_{\text{Monomer B}}$	−532.7	−531.4	−530.4	−531.5 ± 0.7
		W_{Dimer}	−1078.6	−1078.6	−1078.4	−1078.5 ± 0.1
		ΔW_{ass}			**−17.1**±0.7	
	Longer simulations	$W_{\text{Monomer A}}$	−529.8	−531.1	−531.2	−530.7 ± 0.4
		$W_{\text{Monomer B}}$	−531.2	−530.8	−531.2	−531.1 ± 0.2
		W_{Dimer}	−1075.5	−1078.6	−1077.5	−1077.2 ± 0.9
		ΔW_{ass}			**−15.4**±1.0	
GpA15p11	1-ns simulations	$W_{\text{Monomer A}}$	−472.0	−471.5	−470.7	−471.4 ± 0.4
		$W_{\text{Monomer B}}$	−466.8	−468.6	−471.4	−468.9 ± 1.4
		W_{Dimer}	−963.0	−961.7	−963.5	−962.8 ± 0.5
		ΔW_{ass}			**−22.4**±1.5	
	5-ns simulations	$W_{\text{Monomer A}}$	−470.3	−471.6	−470.4	−470.8 ± 0.4
		$W_{\text{Monomer B}}$	−470.1	−471.0	−470.7	−470.6 ± 0.2
		W_{Dimer}	−961.7	−961.7	−961.1	−961.5 ± 0.2
		ΔW_{ass}			**−20.1**±0.5	
	10-ns simulations	$W_{\text{Monomer A}}$	−469.9	N/A	N/A	N/A
		$W_{\text{Monomer B}}$	−470.6	N/A	N/A	N/A
		W_{Dimer}	−961.1	N/A	N/A	N/A
		ΔW_{ass}			**−20.6**	
MCP	1-ns simulations	$W_{\text{Monomer A}}$	−586.4	−588.7	−585.2	−586.8 ± 1.0
		$W_{\text{Monomer B}}$	−585.1	−587.3	−584.0	−585.5 ± 1.0
		W_{Dimer}	−1187.4	−1189.8	−1191.7	−1189.6 ± 1.2
		ΔW_{ass}			**−17.4**±1.9	
	Longer simulations	$W_{\text{Monomer A}}$	−586.3	−586.7	−586.2	−586.4 ± 0.2
		$W_{\text{Monomer B}}$	−585.5	−586.0	−585.4	−585.6 ± 0.2
		W_{Dimer}	−1190.7	−1190.2	−1193.4	−1191.4 ± 1.0
		ΔW_{ass}			**−19.4**±1.0	
MCP-GpA	1-ns simulations	$W_{\text{Monomer A}}$	−588.5	−588.5	−590.2	−589.1 ± 0.5
		$W_{\text{Monomer B}}$	−591.1	−586.1	−592.3	−589.8 ± 1.9
		W_{Dimer}	−1200.4	−1205.3	−1204.8	−1203.5 ± 1.6
		ΔW_{ass}			**−24.6**±2.5	
	Longer simulations	$W_{\text{Monomer A}}$	−588.5	−587.9	−589.0	−588.5 ± 0.3
		$W_{\text{Monomer B}}$	−589.9	−587.6	−589.9	−589.1 ± 0.8
		W_{Dimer}	−1203.9	−1204.0	−1206.5	−1204.8 ± 0.8
		ΔW_{ass}			**−27.2**±1.2	

The temperature T is 298.15 K.

at the binding interface; 2), flanking polar residues can affect association affinity via direct interactions.

Noninterfacial residues in the putative TM domain can affect the association affinity because the extent of their burial in the membrane could be different in monomers and dimers. The effect is particularly strong for charged residues, which need to be as exposed to water as possible. In the case of MCP and MCP-GpA, this is difficult because the tilt and orientation of helices in the dimer are highly constrained by the interhelical interactions, and thus, two Lys-40 side chains in the dimeric structure are forced to point toward the membrane's hydrophobic core. Translation of the protonated dimer downward to expose Lys-40 to the headgroup region is prevented by the unfavorable burial of Tyr-24 on the other end. However, the protonated monomer is not subject to such constraints and can adopt an orientation in which the Tyr-24 side chain points up and the Lys-40 side chain points down (Fig. 2). This allows the helix to translate ~3.9 Å down toward the C-terminus compared with the deprotonated dimer (Table 3) and expose Lys-40 to the headgroup region (Fig. 2). Deprotonation of Lys-40 makes dimerization possible, but at a significant free energy cost. The coupling of protonation/deprotonation and oligomerization has been observed in artificially designed pLeu peptides (43,44), M2 protein (45), and bacterioopsin (46). The energy cost of deprotonation for MCP and MCP-GpA is consistent with these experimental studies and could be the major reason why the association affinity of MCP and MCP-GPA is weaker than that of GpA15p11. Consideration of the heterogeneous membrane environment and how the monomers or oligomers fit into it is essential for a full understanding of binding affinity in transmembrane systems. These calculations suggest that replacing Lys-40 by a polar or, even better, a nonpolar residue should increase binding affinity.

Polar residues in TM helices have been found to influence their association when located in the membrane interior (47–50). It should not then be surprising that they can also do so when they are located in the juxtamembrane region. After the TM 13-residue LIxxGVxxGVxxT motif was first identified, few efforts were made to study the residues outside this motif. Moreover, different flanking residues were systematically introduced in ToxR′ and ToxCAT assays, but their role has not been discussed. Although information about flanking residues in ToxR′ and ToxCAT is not always provided, most studies employed an asparagine consecutive to an arginine at the N-terminal flank of the TM domain. Our study demonstrated that these two residues (Asn-1 and Arg-2) could produce strong interhelical interaction by forming H-bonds when they are three and two residues away from the 13-residue interfacial core. The observation that GpA TM helices seem to associate more strongly in the membrane than in micelles (13,15) could potentially be caused by the flanking residues rather than differences in the environment. SDS-PAGE experiments used the wild-type sequence (as in GpA29 in our study), whereas in vivo experiments used nonnative flanking residues such as GpA15p11 in our study.

Besides the type of flanking residues, their position with respect to the GxxxG motif also affects association affinity. This effect can explain several experimental observations. Langosch et al. (13) found that when the full 13-residue motif was inserted between the N-terminal and C-terminal flanking sequences, NRAS and ILINP, respectively, it gave the strongest dimerization signal compared with insertion of 12 and 14 residues. The reason for this could be that both the addition of one residue at the N-end and the deletion of one residue from the C-end of the 13-residue motif shift the position of the polar residues at the N- and C- flanks and affect the formation of hydrogen bonds between the helices. Johnson et al. (51) studied the effect of GxxxG position on the dimer affinity and have shown that the association in ToxCAT tests is stronger when the GxxxG motif is eight residues away from the N-terminal flank compared with that when it is 12 residues away. Besides the position of GxxxG in the membrane, its position relative to the flanking residues is shifted, which may cause a change of interhelical interactions between the flanking residues. Alternatively, the position of the GxxxG motif could influence the relative orientation of the ToxR domains and thus the measured signal. It is for this possibility that Melnyk et al. constructed MCP-GpA (30). Complete discrimination between the various proposed mechanisms can be done with further experimentation combined with modeling. For example, experimental mutation studies focused on the flanking residues could prove or disprove their contribution to TM helix association affinity.

This study was carried out using an approximate, implicit membrane model that lacks detailed interactions between proteins and water or lipid molecules. This forces us to view the quantitative aspects with some reservations. Because the structurally or functionally meaningful TM helix association is always specific and sequence-dependent, treating the water and lipid molecules implicitly seems acceptable. Although simulations of peptides in explicit lipid bilayers are possible, calculating thermodynamic properties of association and contributions of specific residues does not seem feasible at this point. In addition, the slow equilibration of explicit simulations would introduce a lot of uncertainty in the results. One major source of concern is the assumption of a flat, nondeformable hydrophobic slab. Recent work has shown that the burial of charged or highly polar side chains leads to membrane deformations and water defects (52). An adaptation of the continuum electrostatics method that takes these effects into account has been developed (53) but is not appropriate for MD simulations. IMM1 does not explicitly account for water defects and membrane deformations, but the choice of solvation parameters may give results that are comparable to those obtained from explicit simulations. For example, in our model the transfer free energies of the protonated and deprotonated Lys side

chains from water to the membrane interior are 14.49 kcal/mol and −0.06 kcal/mol, respectively. (These values were calculated by summing up the transfer free energies of all groups composing Lys+ or Lys; see Table II of Lazaridis (33)). The value for protonated Lys is much smaller than one would get using the Born model. However, this value is not far from what is observed in explicit simulations because of the membrane adjustments or water defects mentioned above (52,54). Recent calculations of the potential of mean force needed to transfer a charged Arg side chain from water to the membrane core by MD simulations with an explicit membrane yielded the value ~17 kcal/mol (55). The transfer free energy of the protonated Arg side chain from water to the membrane interior in our model is 20.67 kcal/mol, quite close to the above value.

There is also some uncertainty with the Arg parameterization at the membrane interface. We have found evidence suggesting that the Arg-Arg interaction should be more repulsive than predicted by IMM1 (25). In our calculations there were no Arg pairs interacting, but a pair of Asn and Arg in GpA15p11 was found to favorably contribute 2.7 kcal/mol to the interhelical interactions. This value seems reasonable but should be treated with some caution.

One final source of uncertainty is that the structure of MCP is putative. The stability of these putative structures under MD simulations and the good agreement with the relative affinities obtained by ToxCAT experiments lends some support to the structures proposed by Melnyk et al. (30)

Our findings could be tested by the following experiments: 1), insertion of one or a few residues between the nonnative flanking residues and the 13-residue association core in the sequence of GpA15p11 should decrease the association affinity; 2), mutation of Lys-40 on MCP and MCP-GpA to a hydrophobic residue or even a less polar residue should increase the association affinity; and 3), high pH should also increase the association affinity by lessening the cost of deprotonating Lys.

We thank Dr. M. Mihajlovic and Dr. C.M. Deber for helpful discussions. This work was supported by the National Science Foundation (MCB-0316667).

Infrastructure support was provided in part by Research Centers in Minority Institutions grant RR03060 from the National Institutes of Health.

REFERENCES

1. Popot, J. L., and D. M. Engelman. 1990. Membrane protein folding and oligomerization: the two-stage model. *Biochemistry*. 29:4031–4037.
2. Engelman, D. M., Y. Chen, C. N. Chin, A. R. Curran, A. M. Dixon, et al. 2003. Membrane protein folding: beyond the two stage model. *FEBS Lett*. 555:122–125.
3. Matthews, E. E., M. Zoonens, and D. M. Engelman. 2006. Dynamic helix interactions in transmembrane signaling. *Cell*. 127:447–450.
4. von Heijne, G. 2007. The membrane protein universe: what's out there and why bother? *J. Intern. Med*. 261:543–557.
5. Yin, H., J. S. Slusky, B. W. Berger, R. S. Walters, G. Vilaire, et al. 2007. Computational design of peptides that target transmembrane helices. *Science*. 315:1817–1822.
6. Lemmon, M. A., J. M. Flanagan, H. R. Treutlein, J. Zhang, and D. M. Engelman. 1992. Sequence specificity in the dimerization of transmembrane alpha-helices. *Biochemistry*. 31:12719–12725.
7. Lemmon, M. A., J. M. Flanagan, J. F. Hunt, B. D. Adair, B. J. Bormann, et al. 1992. Glycophorin A dimerization is driven by specific interactions between transmembrane alpha-helices. *J. Biol. Chem*. 267:7683–7689.
8. Fleming, K. G., A. L. Ackerman, and D. M. Engelman. 1997. The effect of point mutations on the free energy of transmembrane alpha-helix dimerization. *J. Mol. Biol*. 272:266–275.
9. Fleming, K. G. 2002. Standardizing the free energy change of transmembrane helix-helix interactions. *J. Mol. Biol*. 323:563–571.
10. Fleming, K. G., C. C. Ren, A. K. Doura, M. E. Eisley, F. J. Kobus, et al. 2004. Thermodynamics of glycophorin A transmembrane helix dimerization in C14 betaine micelles. *Biophys. Chem*. 108:43–49.
11. Fisher, L. E., D. M. Engelman, and J. N. Sturgis. 1999. Detergents modulate dimerization, but not helicity, of the glycophorin A transmembrane domain. *J. Mol. Biol*. 293:639–651.
12. Fisher, L. E., D. M. Engelman, and J. N. Sturgis. 2003. Effect of detergents on the association of the glycophorin a transmembrane helix. *Biophys. J*. 85:3097–3105.
13. Langosch, D., B. Brosig, H. Kolmar, and H. J. Fritz. 1996. Dimerisation of the glycophorin A transmembrane segment in membranes probed with the ToxR transcription activator. *J. Mol. Biol*. 263:525–530.
14. Brosig, B., and D. Langosch. 1998. The dimerization motif of the glycophorin A transmembrane segment in membranes: importance of glycine residues. *Protein Sci*. 7:1052–1056.
15. Russ, W. P., and D. M. Engelman. 1999. TOXCAT: a measure of transmembrane helix association in a biological membrane. *Proc. Natl. Acad. Sci. USA*. 96:863–868.
16. Finger, C., T. Volkmer, A. Prodohl, D. E. Otzen, D. M. Engelman, et al. 2006. The stability of transmembrane helix interactions measured in a biological membrane. *J. Mol. Biol*. 358:1221–1228.
17. Russ, W. P., and D. M. Engelman. 2000. The GxxxG motif: a framework for transmembrane helix-helix association. *J. Mol. Biol*. 296:911–919.
18. Lemmon, M. A., H. R. Treutlein, P. D. Adams, A. T. Brunger, and D. M. Engelman. 1994. A dimerization motif for transmembrane alpha-helices. *Nat. Struct. Biol*. 1:157–163.
19. Senes, A., M. Gerstein, and D. M. Engelman. 2000. Statistical analysis of amino acid patterns in transmembrane helices: the GxxxG motif occurs frequently and in association with beta-branched residues at neighboring positions. *J. Mol. Biol*. 296:921–936.
20. MacKenzie, K. R., J. H. Prestegard, and D. M. Engelman. 1997. A transmembrane helix dimer: structure and implications. *Science*. 276:131–133.
21. Smith, S. O., D. Song, S. Shekar, M. Groesbeek, M. Ziliox, et al. 2001. Structure of the transmembrane dimer interface of glycophorin A in membrane bilayers. *Biochemistry*. 40:6553–6558.
22. Senes, A., I. Ubarretxena-Belandia, and D. M. Engelman. 2001. The Calpha—H…O hydrogen bond: a determinant of stability and specificity in transmembrane helix interactions. *Proc. Natl. Acad. Sci. USA*. 98:9056–9061.
23. Arbely, E., and I. T. Arkin. 2004. Experimental measurement of the strength of a C alpha-H…O bond in a lipid bilayer. *J. Am. Chem. Soc*. 126:5362–5363.
24. Mottamal, M., and T. Lazaridis. 2005. The contribution of C alpha-H…O hydrogen bonds to membrane protein stability depends on the position of the amide. *Biochemistry*. 44:1607–1613.
25. Mottamal, M., J. Zhang, and T. Lazaridis. 2006. Energetics of the native and non-native states of the glycophorin transmembrane helix dimer. *Proteins*. 62:996–1009.
26. Lomize, A. L., I. D. Pogozheva, and H. I. Mosberg. 2004. Quantification of helix-helix binding affinities in micelles and lipid bilayers. *Protein Sci*. 13:2600–2612.
27. Zhang, J., and T. Lazaridis. 2006. Calculating the free energy of association of transmembrane helices. *Biophys. J*. 91:1710–1723.

28. Kim, S., T. J. Jeon, A. Oberai, D. Yang, J. J. Schmidt, et al. 2005. Transmembrane glycine zippers: physiological and pathological roles in membrane proteins. *Proc. Natl. Acad. Sci. USA*. 102:14278–14283.

29. Fleming, K. G., and D. M. Engelman. 2001. Specificity in transmembrane helix-helix interactions can define a hierarchy of stability for sequence variants. *Proc. Natl. Acad. Sci. USA*. 98:14340–14344.

30. Melnyk, R. A., S. Kim, A. R. Curran, D. M. Engelman, J. U. Bowie, et al. 2004. The affinity of GXXXG motifs in transmembrane helix-helix interactions is modulated by long-range communication. *J. Biol. Chem.* 279:16591–16597.

31. Doura, A. K., F. J. Kobus, L. Dubrovsky, E. Hibbard, and K. G. Fleming. 2004. Sequence context modulates the stability of a GxxxG-mediated transmembrane helix-helix dimer. *J. Mol. Biol.* 341:991–998.

32. Doura, A. K., and K. G. Fleming. 2004. Complex interactions at the helix-helix interface stabilize the glycophorin A transmembrane dimer. *J. Mol. Biol.* 343:1487–1497.

33. Lazaridis, T. 2003. Effective energy function for proteins in lipid membranes. *Proteins.* 52:176–192.

34. Lazaridis, T. 2005. Implicit solvent simulations of peptide interactions with anionic lipid membranes. *Proteins.* 58:518–527.

35. Lazaridis, T., and M. Karplus. 1999. Effective energy function for proteins in solution. *Proteins*. 35:133–152.

36. van Klompenburg, W., and B. de Kruijff. 1998. The role of anionic lipids in protein insertion and translocation in bacterial membranes. *J. Membr. Biol.* 162:1–7.

37. Boon, J. M., and B. D. Smith. 2002. Chemical control of phospholipid distribution across bilayer membranes. *Med. Res. Rev.* 22:251–281.

38. Matsuzaki, K. 1999. Why and how are peptide-lipid interactions utilized for self-defense? Magainins and tachyplesins as archetypes. *Biochim. Biophys. Acta.* 1462:1–10.

39. Dawson, J. P., R. A. Melnyk, C. M. Deber, and D. M. Engelman. 2003. Sequence context strongly modulates association of polar residues in transmembrane helices. *J. Mol. Biol.* 331:255–262.

40. Melnyk, R. A., A. W. Partridge, and C. M. Deber. 2002. Transmembrane domain mediated self-assembly of major coat protein subunits from Ff bacteriophage. *J. Mol. Biol.* 315:63–72.

41. Mihajlovic, M., and T. Lazaridis. 2006. Calculations of pH-dependent binding of proteins to biological membranes. *J. Phys. Chem. B*. 110: 3375–3384.

42. Vos, W. L., R. B. Koehorst, R. B. Spruijt, and M. A. Hemminga. 2005. Membrane-bound conformation of M13 major coat protein: a structure validation through FRET-derived constraints. *J. Biol. Chem.* 280: 38522–38527.

43. Lew, S., J. Ren, and E. London. 2000. The effects of polar and/or ionizable residues in the core and flanking regions of hydrophobic helices on transmembrane conformation and oligomerization. *Biochemistry.* 39: 9632–9640.

44. Lew, S., G. A. Caputo, and E. London. 2003. The effect of interactions involving ionizable residues flanking membrane-inserted hydrophobic helices upon helix-helix interaction. *Biochemistry*. 42:10833–10842.

45. Salom, D., B. R. Hill, J. D. Lear, and W. F. DeGrado. 2000. pH-dependent tetramerization and amantadine binding of the transmembrane helix of M2 from the influenza A virus. *Biochemistry*. 39:14160–14170.

46. Valluru, N., F. Silva, M. Dhage, G. Rodriguez, S. R. Alloor, et al. 2006. Transmembrane helix-helix association: relative stabilities at low pH. *Biochemistry*. 45:4371–4377.

47. Zhou, F. X., M. J. Cocco, W. P. Russ, A. T. Brunger, and D. M. Engelman. 2000. Interhelical hydrogen bonding drives strong interactions in membrane proteins. *Nat. Struct. Biol.* 7:154–160.

48. Zhou, F. X., H. J. Merianos, A. T. Brunger, and D. M. Engelman. 2001. Polar residues drive association of polyleucine transmembrane helices. *Proc. Natl. Acad. Sci. USA*. 98:2250–2255.

49. Choma, C., H. Gratkowski, J. D. Lear, and W. F. DeGrado. 2000. Asparagine-mediated self-association of a model transmembrane helix. *Nat. Struct. Biol.* 7:161–166.

50. Gratkowski, H., J. D. Lear, and W. F. DeGrado. 2001. Polar side chains drive the association of model transmembrane peptides. *Proc. Natl. Acad. Sci. USA*. 98:880–885.

51. Johnson, R. M., A. Rath, and C. M. Deber. 2006. The position of the Gly-xxx-Gly motif in transmembrane segments modulates dimer affinity. *Biochem. Cell Biol.* 84:1006–1012.

52. MacCallum, J. L., W. F. Bennett, and D. P. Tieleman. 2007. Partitioning of amino acid side chains into lipid bilayers: results from computer simulations and comparison to experiment. *J. Gen. Physiol.* 129:371–377.

53. Choe, S., K. A. Hecht, and M. Grabe. 2008. A continuum method for determining membrane protein insertion energies and the problem of charged residues. *J. Gen. Physiol.* 131:563–573.

54. Freites, J. A., D. J. Tobias, G. von Heijne, and S. H. White. 2005. Interface connections of a transmembrane voltage sensor. *Proc. Natl. Acad. Sci. USA*. 102:15059–15064.

55. Dorairaj, S., and T. W. Allen. 2007. On the thermodynamic stability of a charged arginine side chain in a transmembrane helix. *Proc. Natl. Acad. Sci. USA*. 104:4943–4948.